Proceedings of the ASME 2010 3rd Joint US-European Fluids Engineering Summer Meeting and 8th International Conference on Nanochannels, Microchannels, and Minichannels
FEDSM-ICNMM2010
August 1-5, 2010, Montreal, Canada

FEDSM-ICNMM2010-30215

SELF-SUSTAINED OSCILLATIONS OF HIGH SPEED IMPINGING PLANAR JETS

David Arthurs
McMaster University
Hamilton, Ontario, Canada
arthurdg@mcmaster.ca

Samir Ziada
McMaster University
Hamilton, Ontario, Canada
ziadas@mcmaster.ca

ABSTRACT

High speed impinging jets are frequently used in a variety of industrial applications including thermal and coating control processes. These flows are liable to the production of very intense narrow band acoustic tones, which are produced by a feedback mechanism between instabilities in the jet free shear layer which roll up to form large scale coherent structures, and pressure fluctuations produced by the impingement of these structures at the impingement surface. This paper examines tone generation of a high speed planar gas jet impinging normally on a flat, rigid surface. Experiments are performed over the complete range of subsonic and transonic jet flow velocities for which tones are generated, from U_o=150m/s (M≈0.4) to choked flow (U_o=343m/s, M=1), and over the complete range of impingement distance for which tones occur. The effect of varying the jet thickness is also examined. The behavior of the planar impinging jet case is compared to that of the axisymmetric case, and found to be significantly different, with tones being excited at larger impingement distances, and at lower flow velocities. The Strouhal numbers associated with tone generation in the planar case are on average an order of magnitude lower than that of the axisymmetric case when using similar velocity and length scales. The frequency behavior of the resulting tones is predicted using a simple feedback model, which allows the identification of the various shear layer modes of the instabilities driving tone generation. Finally, a thorough dimensionless analysis is performed in order to quantify the system behavior in terms of the appropriate scales.

INTRODUCTION

High speed impinging jet flows are known to be liable to excitation of very intense acoustic tones generated by a feedback mechanism between instabilities in the free shear layer of the jet, and large pressure fluctuations produced by the flow at the impingement surface. These effects can limit the usefulness of this geometry in many applications, however recent research by O'Donovan & Murray [1-2] has shown that local heat transfer rates for impinging jets can be enhanced by as much as 30% by *inducing* tone generation. Various forms of impinging jet flows have been the subject of a relatively intense research effort in the literature. The various forms which have been investigated to date can be broadly grouped as those using axisymmetric jets, and those using planar jets.

Of the geometries consisting of jets impinging on flat rigid surfaces, the majority of the research in the literature has been devoted to the axisymmetric case. Various aspects of the feedback excitation mechanism for the subsonic axisymmetric case have been investigated by Ho & Nossier [3], Nossier & Ho [4], Tam & Ahuja [5] and Panickar & Raman [6], among many others. Extensive work on the axisymmetric case involving supersonic flows has been performed such as Henderson & Powell [7], Krothapelli et al. [8] and Henderson [9]. In addition, the planar impinging jet case using supersonic jets has also received some attention in the literature, e.g Krothapelli [10] and others. In comparison to axisymmetric jets, the impinging planar jet case using *subsonic* flows has received relatively little attention in the literature, despite being widely used in a myriad of practical and industrial applications such as thermal processing in both heating and cooling applications, the production of sheet glass and polymer films, coating control applications, among others.

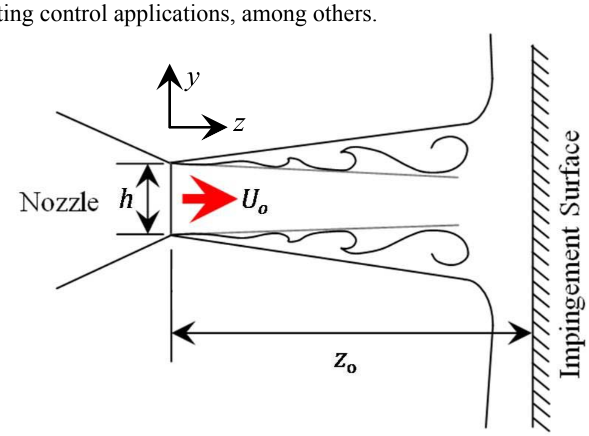

Figure 1: Basic schematic of the impinging planar jet geometry, showing the initial jet flow velocity (Uo), the impingement distance (zo) and the nozzle slot width, as well as the downstream (z) and cross-stream (y) directions.

There has also been considerable work performed on *similar* geometries which use impinging planar jets, such as the jet-edge and jet-slot systems. Two recent studies examining the jet-slot system are Billon et al. [11] and Glesser et al. [12] which examined the coupling of a planar jet-slot oscillator with longitudal modes of the flow supply duct for Mach numbers up to M=0.1. In addition, there are many other examples in the literature documenting the response of the jet-slot oscillator such as Rockwell & Naudascher [13], Ziada [14] and Ziada, [15]. There are also numerous examples of work performed on the jet-edge system such as Powell [16], Karamacheti et al. [17], Ziada [18] and Ziada & Rockwell [19]. The response of the jet-edge and jet-slot systems is in some respects similar to the response of the planar jet impinging normally on flat, rigid surfaces; however the range of flow velocity and impingement distance varies from these cases substantially.

The current study focuses on experimental results of a high speed, subsonic planar jet impinging normally on a flat surface. A parametric study has been performed in which the impingement distance (z_o), jet slot width (h) and incident velocity (U_o) have been varied.

NOMENCLATURE

c_a Speed of sound in air
d Distance of the microphone from the impingement point
D Nozzle diameter of an impinging axisymmetric jet
f Frequency
h Nozzle slot width
L Length of the planar jet in the span-wise direction
L/h Nozzle aspect ratio
M Mach number (U_o/c_a)
P Plenum pressure
P_t Total pressure
Re_h Reynolds number based upon jet slot width ($U_o \cdot h/\nu$)
SPL Sound pressure level in decibels [$20 \cdot \log_{10}(P_{RMS}/P_{ref})$ *where* P_{ref}=20μPa]
St_{zo} Strouhal number ($f \cdot z_o/U_o$)
U_c Convection speed
U_d Velocity scale of the downstream portion of the feedback mechanism.
U_o Jet velocity at the centerline of the nozzle outlet
U_u Velocity scale of the upstream portion of the feedback mechanism.
z_o The impingement distance (distance from the edge of the nozzle to the impingement surface).
z_o/h Impingement ratio
θ Angle of microphone as measured from the impingement plane

EXPERIMENTAL APPARATUS

Experiments were performed using the apparatus shown in Figure 2. The nozzle was constructed using aluminum, and uses an elliptical nozzle profile to provide a top-hat shaped velocity profile with thin shear layers at the nozzle exit. The plenum of the nozzle contains several flow conditioning devices to evenly distribute the flow along the jet span, and reduce the turbulence intensity at the nozzle exit. A perforated tube is mounted inside the plenum to receive the flow entering the plenum from one end and distribute it radially outward. This tube has holes of varying size along its length to distribute the flow outward, evenly along its length.

In addition, two screens are mounted immediately upstream of the nozzle contraction to break up large scale turbulent structures in the plenum. The screens are a fine mesh with 70 wires/inch and an open area ratio of β=0.55. The plenum, nozzle contraction profile, and flow conditioners were designed using a commercial CFD package, and thorough testing has been performed to ensure that flow exiting the nozzle was evenly distributed and had the desired top-hat shaped velocity profile. The jet nozzle also allows for the adjustment of the jet slot width (h) from h=1mm to h=6mm in increments of 0.25mm, however for the current study only cases with h=1, 2, 3mm will be presented. The overall span of the jet is L=100mm, resulting in an aspect ratio of the planar nozzle of between L/h=100 and L/h=33.3, depending on the jet slot width tested.

The impingement surface consists of a 12mm thick aluminum plate, which has been machined to provide a smooth, flat surface. The impingement surface is held in place using an assembly which also allows for the effects of plat inclination to be tested, however those effects will not be covered in this study. The jet nozzle and impingement surface assemblies are mounted to a pair of precision rotary stages, and then to a pair of linear manual traverses. The traverse holding the jet nozzle is oriented in the z-direction (downstream direction), while the traverse and rotary stage holding the impingement surface assembly is oriented in the y-direction (cross-stream direction). The precision rotary stages have a fine adjustment with a Vernier scale and can control the angle of the impinging jet or the impingement surface to within 0.1°, while the linear traverses have a resolution of 0.02mm.

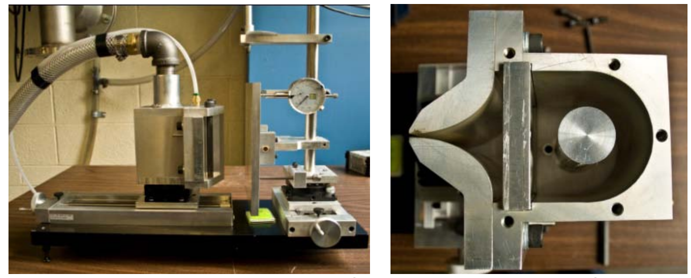

Figure 2: Photographs of the apparatus used for experimental testing (a) Nozzle and plate assemblies showing manual traverses oriented in the y and z-directions and precision rotary stages. (b) Internal geometry of the planar nozzle showing the flow distribution tube, flow conditioning screens and elliptical nozzle profile.

The jet nozzle is pressurized using compressed air, with the plenum pressure being controlled by a gate valve located well upstream of the plenum. The plenum pressure is monitored using a Validyne DP15 pressure transducer with a -42 diaphragm, enabling pressure measurements up to P=2.4bar (absolute pressure). The location of the pressure measurement is immediately downstream of the last flow conditioning screen prior to the nozzle contraction. For the current study, plenum pressures of P=1.13 bar up to P=1.89 bar (*absolute pressure*) have been tested corresponding to flow velocities at the centerline of the jet nozzle of U_o=150m/s up to U_o=343m/s (*choked flow*). The flow velocity of the exiting jet is estimated using the flowing relation derived for flow exiting an isentropic nozzle:

$$U_o = c_a \sqrt{\frac{2}{\gamma - 1}\left[\left(\frac{P}{P_\infty}\right)^{\left(\frac{\gamma-1}{\gamma}\right)} - 1\right]} \tag{1}$$

where U_o is the flow velocity exiting at the jet centerline, P is the plenum pressure, P_∞ is the ambient pressure and c_a is the speed of sound.

Measurements of the velocity profiles, as shown in Figure 3, at the nozzle exit have been performed for a series of jet slot widths and flow velocities, both in the y-direction, across the jet slot width, and in the span-wise x-direction, to ensure even flow distribution along the jet span. The velocity measurements have been performed using miniature pressure probe constructed using stainless steel hypodermic tubing. The probe tip was constructed using a 32-guage medical needle with an outer diameter of $ø_o$=0.23 mm. The measurement surface was created by pinching and cutting the tube, and then filing the front and side surfaces to create an aerodynamically shaped tip. The front surface was carefully filed until an opening to the tube in the shape of a long thin slot was revealed. The thickness, δ, of the slot-shaped opening was measured optically and was found to be δ≈0.01mm, while the length of the slot was found to be ε≈0.14 mm. The direction of the slot was aligned with the x-direction of the jet, i.e. along the span-wise direction of the jet, where there are no appreciable variations in the mean flow. The 32 gauge tubing forms the initial 4mm of the overall probe length, after which the smaller diameter tube was soldered to the 20 gauge tubing to add extra rigidity. Finally, the 20 gauge tubing was attached to a manual traverse mechanism via a thin, aerodynamically shaped support which allowed placement of the probe within the flow field with an accuracy of 0.02mm.

The pressure probe has been designed to measure the total pressure of the flow, at the tip of the probe where the flow is brought to rest. This measurement procedure is based on the assumption that the flow is halted isentropically, which is the same assumption made in a standard pitot tube. The flow velocity A measurement of the flow can be made at each measurement point can be estimated using the expression:

$$u(y) = c_a \sqrt{\frac{2}{\gamma - 1}\left[\left(\frac{P_t}{P_\infty}\right)^{\left(\frac{\gamma-1}{\gamma}\right)} - 1\right]} \qquad (2)$$

where P_t is the total pressure. This expression is essentially identical to Equation (1) given earlier, and the assumption and implications are the same as well, but has simply been adapted to be used for point measurements.

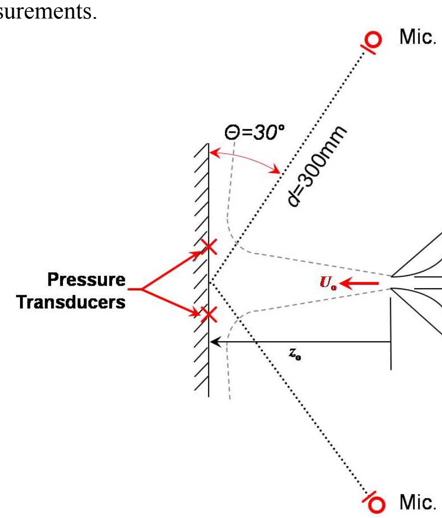

Figure 4: Basic schematic of the layout of instrumentation showing two microphones in the acoustic far-field and flush mounted pressure transducers at the plate surface.

The pressure probes were developed as a result of great difficulty in obtaining velocity measurements using hot-wire anemometry, specifically with challenges involving probe breakage due to the very high flow velocities, large velocity gradients, and compensation of differences between the jet and ambient temperatures. There are expected to be some ill effects due to the nature of the velocity measurement using a probe of this type, specifically that fluctuations in pressure at the probe tip may not be measured in a perfectly linear fashion, with some hysteresis due to the small opening, which may in turn cause an overestimation of the flow velocity in areas where the turbulence intensity is significant. All measurements made using these probes have been performed at the nozzle outlet, where the turbulence intensities are relatively low. However, in the shear layer, the turbulence intensities can approach 50% or more, and the non-linearity of the measurement may produce an artificial thinning of the shear layer thicknesses (Hinze, [20]). Despite these drawbacks, the measurements are expected to provide reasonable estimates of the exiting jet profiles.

Acoustic measurements in the free field were performed using two GRAS ¼" pressure microphones, with a flat frequency response up to 70kHz (+/-2dB). The microphones were mounted using a set of adjustable rigid mounts which allowed the adjustment of the position of the microphone. In addition, a pair of miniature piezoelectric pressure transducers with a flat frequency response up to 200kHz were flush mounted to the plate surface in a symmetric pattern on either side of the centerline of the impinging planar jet. Data was acquired using Labview at a sample rate of 50kHz with a bin size of 25,000 samples for 30 seconds per measurement. The time series was used to construct spectra of the signals using 30 averages with 1 second of data for each average, and no overlap. The resulting spectra have a frequency range of 0-25kHz, and a frequency resolution of 2Hz.

As all acoustics measurements were performed in a non-anechoic environment, care was taken to ensure that measurements were not performed in the reverberant field. Figure 5 shows the overall sound pressure levels as a function of microphone distance for a impinging planar jet configuration with a strong acoustic tone at approximately 5kHz. The microphone distance (*d*) is measured from the impingement point to microphone diaphragm and the estimated resolution in microphone placement is +/-1mm in the three principal directions.

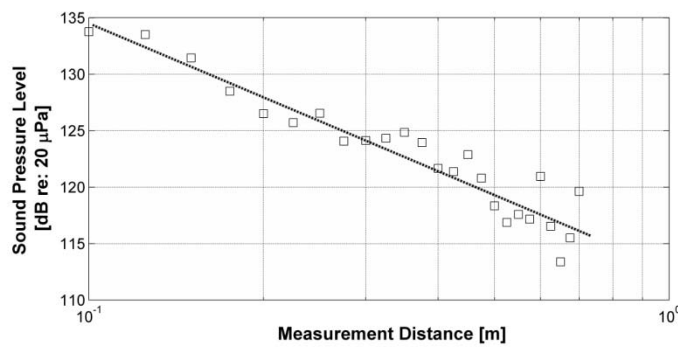

Figure 5: Overall Sound pressure level as a function of microphone distance (*d*) for an impinging planar jet configuration with U_o= 205m/s, z_o/h=10, and *h*=2mm and θ=30°.

As can be seen in Figure 5, the sound pressure level decays exponentially as a function of the microphone distance, indicating that measurements within this range are not within the reverberant field. All subsequent acoustics measurement were performed at a microphone distance of *d*=300mm and an angle of θ=30°, as measured from the surface of the plate at the impingement point, with the two microphones being placed on either side of the nozzle.

RESULTS

The current analysis is based on a complete set of results in which the experimental parameters were varied within the following ranges. The flow velocity (U_o) was varied from 150m/s, the lowest flow velocity for which tone were excited, up to choked flow (343m/s), in increments of 5m/s, for a total of 40 spectral measurements per test run. The impingement ratio (z_o/h), defined as the ratio of the impingement distance to the jet slot width, has been varied from z_o/h=6 to 30, in increments of 2. For impingement ratios of less than 6, no acoustic tones were observed, and tones were typically observed for a range of impingement ratios from z_o/h=6 to 30, although for specific configurations, tones were generated up to impingement ratios of z_o/h≈45. Three jet slot widths of *h*=1mm, 2mm and 3mm have been tested for each case.

Figure 6 shows a series of acoustic spectra with amplitude shown in sound pressure level (SPL) as defined by Equation (3) for three tone generating configurations. The configurations are for a fixed impingement ratio and jet slot width, with only the flow velocity being changed. The three spectra shown are representative of the acoustic signature of the noise generated by this geometry, with high levels of broadband noise due to the turbulent nature of the jet impingement, and intense acoustic tones in excess of 30dB over broadband levels.

$$SPL = 20 \cdot \log_{10}\left(P_{RMS}/P_{ref}\right)$$
$$where\ \mathrm{P}_{ref} = 20\mu Pa \tag{3}$$

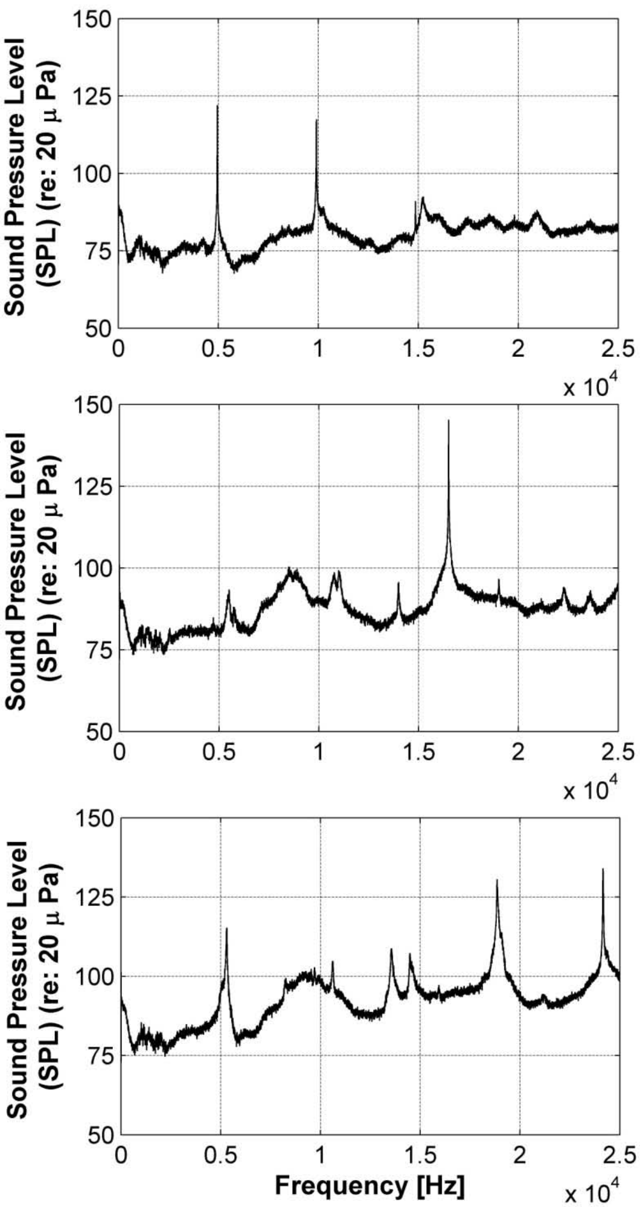

Figure 6: Examples of spectra of sound pressure level recorded by microphones for a planar jet-surface impingement for z_o/h=10, *h*=2mm and (*top plot*) U_o=250m/s, (*middle plot*) U_o=280m/s, (*bottom plot*) U_o=300m/s.

A collection of acoustic spectra for a single experimental run are shown together in a contour plot in Figure 7. The contour plot shows the aeroacoustic response for a single impingement ratio of z_o/h=10 as the flow velocity is varied from U_o=150m/s, the critical flow velocity for this impingement ratio marking the onset of acoustic tone generation, up to choked flow, U_o=343m/s. For this impingement ratio, the acoustic tones are generated in three distinct stages, with each successive jet stage being excited at higher frequencies. In this regard, the response of the planar jet-surface configuration appears qualitatively similar to the axisymmetric impinging jet case, as well as to other more specialized impinging planar jet cases, such as the jet-slot and jet-edge cases. The acoustic tones generated for this geometry are very intense, with maximum tone amplitudes in excess of 145dB for the second jet stage excited for this case at a frequency of *f*=16.5kHz.

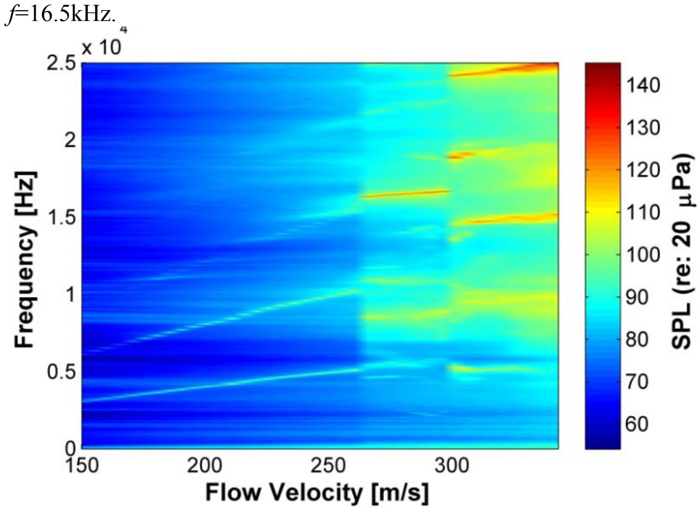

Figure 7: Contour plot of the sound pressure level as a function of the flow velocity for an impingement ratio of z_o/h=10 and *h*=2mm.

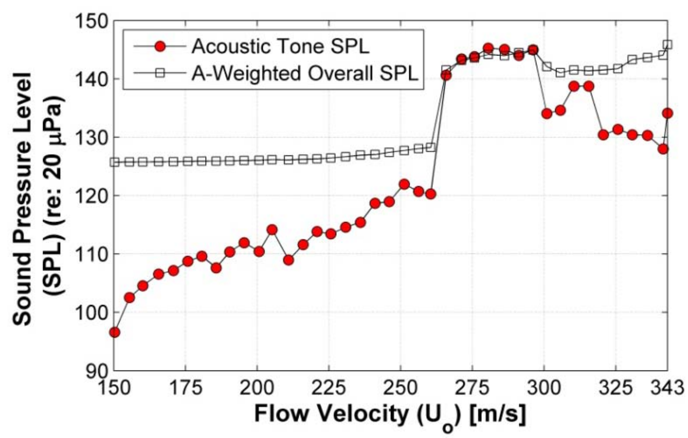

Figure 8: A-weighted overall sound pressure level and Sound pressure level of the dominant acoustic tone as a function of flow velocity for z_o/h=10, *h*=2mm.

Figure 8 shows the sound pressure level of the acoustic tone for each measurement taken in the contour plot, as well as the overall A-weighted sound pressure level. For the flow velocity range where the initial jet stage is excited, between U_o=150m/s and 265m/s, it is evident that the amplitude of the acoustic tone increases with flow velocity, whereas the overall sound pressure levels increase only slightly. For this stage, the tone amplitude approaches nearly 120dB, however, the broadband noise levels are relatively low compared to later jet stages. At the onset of the second jet stage, the amplitude of the tone and broadband levels increase significantly; tone amplitudes reach over 145dB, and there is a discrete jump of more than 10dB in the broadband levels at the onset of this second jet stage. The third excited stage has similarly high broadband noise levels which continue to rise with increasing flow velocity; however the tone amplitudes are not as significant as those in the second stage.

Experimental testing on the impinging planar jet case was performed over a range of impingement ratios, and for three jet slot widths, over a series of experimental runs in which the flow velocity was varied. Figure 9 shows the results of experimental testing performed for a range of impingement ratios from z_o/h=6 to 30 for a fixed jet thickness of h=2mm. In general for all cases, it was found that strong acoustic tones could be excited for impingement ratios from z_o/h=6 to z_o/h=30, and that for small jet slot widths, tones could be excited up to impingement ratios of $z_o/h\approx45$. From inspection of Figure 10, it is relatively clear that the frequency of acoustic tones are approximately proportional to the flow velocity of the impinging jet, and inversely proportional to the impingement ratio.

The configuration most susceptible to tone generation was the impingement ratio case z_o/h=10, with tones being excited at the greatest amplitudes and at the lowest flow velocities. As the impingement ratio increases, the critical flow velocity required to generate acoustic tones also increases, and the maximum amplitude of the acoustic tones decreases. For a jet slot width of h=2mm and an impingement ratio of z_o/h=30, shown in Figure 9, a flow velocity of U_o=290m/s ($M\approx0.85$) is required to generate any audible tones, however strong tones with amplitudes of more than 120dB are excited as the flow velocity is increased to the transonic flow regime (M>0.95).

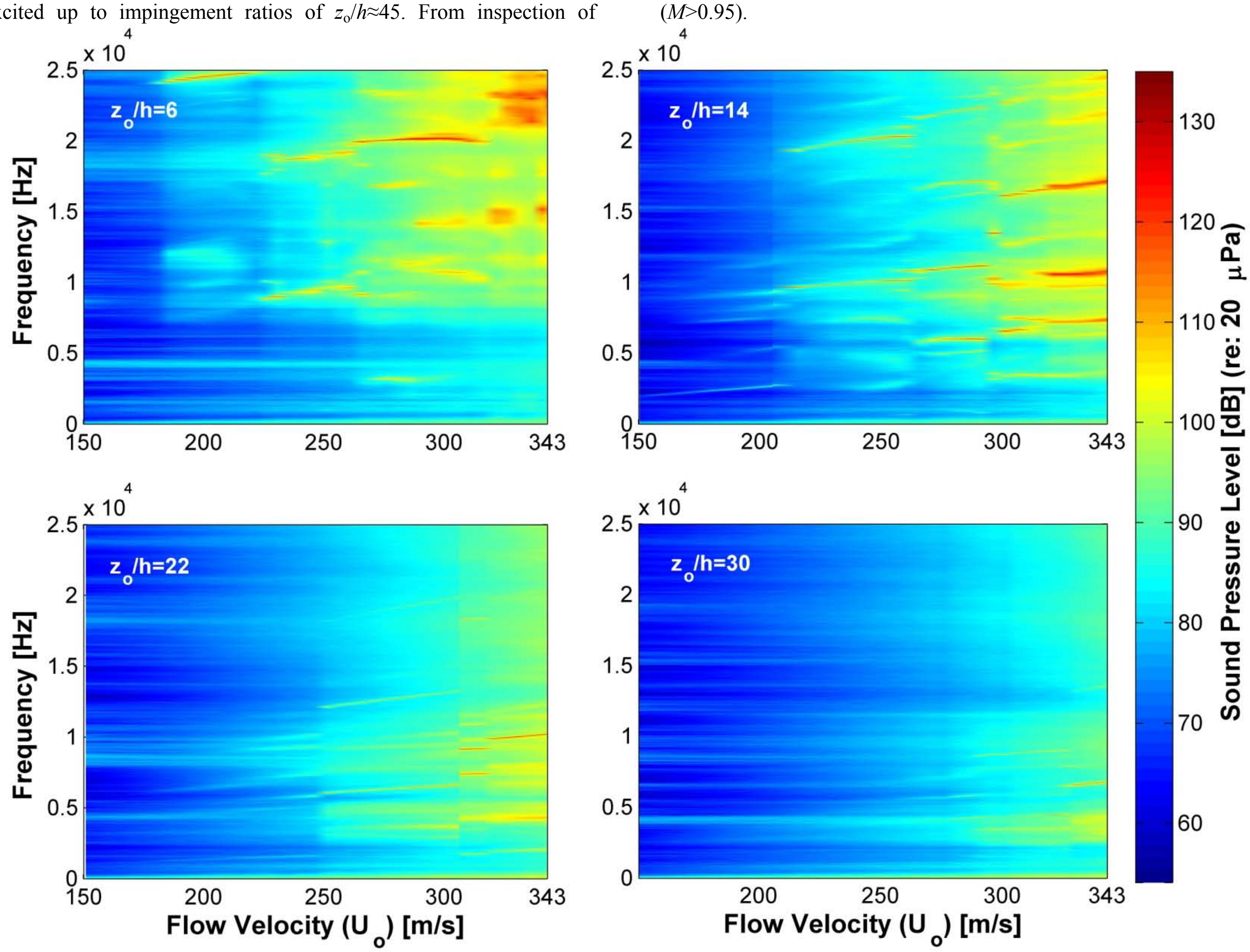

Figure 9: A collection of contour plots showing the sound pressure level as a function of the flow velocity for each case. Contour plots show cases with impingement ratios of z_o/h=6, 14, 22 & 30 respectively and with h=2mm for all cases.

FREQUENCY ANALYSIS

As mentioned previously, the generation of acoustic tones in the planar impinging jet case is qualitatively similar to the axisymmetric impinging jet case, where tones are excited in successive stages, whose frequency is, in general, proportional to flow velocity and inversely proportional to impingement distance. Work performed on the axisymmetric case by previous authors such as Panickar & Raman [6] and Tam & Ahuja [5] have successfully modeled the feedback mechanism generating acoustic tones by adapting a form of the Rossiter model (Rossiter, [21]) which was originally developed for tone generation by high speed flows over shallow cavities. The Rossiter model simply assumes that the feedback mechanism which drives tone generation, consists of the downstream travelling coherent structures in the jet flow, and upstream propagating acoustic pressure fluctuations. The expression, given in Equation (4), is an adaptation of the original model, redeveloped and applied by Panickar & Raman [6] to the impinging axisymmetric jet case. It was used to predict the frequency of acoustic tones generated by the n^{th} shear layer mode of the jet as a function of the jet flow velocity and the impingement distance.

$$f_n = \frac{n \cdot \kappa \cdot U_o \cdot c_a}{z_o \left(\kappa \cdot U_o + c_a \right)} \tag{4}$$

where the coefficient (κ) is the convection coefficient defined as:

$$\kappa = U_c / U_o \tag{5}$$

where U_c is the convection velocity of coherent structures in the jet shear layer. Panickar & Raman [6] found that the use of a single value of convection coefficient of κ=0.65 allowed the best fit with their experimental measurements over a range of impingement ratios from z_o/D=1.5-5.5.

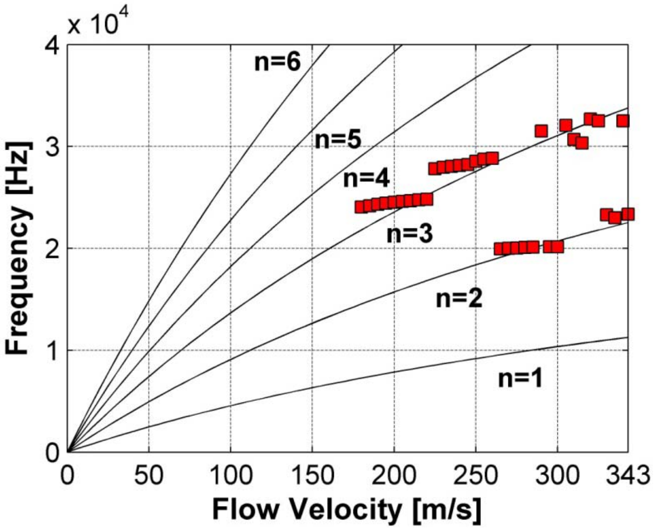

Figure 10: Frequency of the dominant acoustic tone for z_o/h=6 and h=2mm, as a function of flow velocity plotted with the prediction of Equation (4) for the n^{th} Rossiter mode (κ=0.65).

Given the similarities in tone generation mechanism for both the planar and axisymmetric impinging jet cases, a comparison of Panickar & Raman's Rossiter model to the experimentally measured tone frequencies of the planar case for an impingement ratio of z_o/h=6 and h=2mm has been provided in Figure 10. The model presented in the figure uses a convection coefficient of κ=0.65, identical to the coefficient used by Panickar & Raman in their study of the axisymmetric case. This coefficient was applied to the experimental results of the z_o/h=6 impingement ratio case, given that the impingement ratio is only slightly larger than the range defined by the authors for the axisymmetric model, and that the structure of the two flows is expected to be similar for comparable impingement ratios. As can be seen from inspection of the figure, the agreement between the prediction of the model and the measured frequencies is quite good. The model predicts the excitation of the second and third (n=2 & n=3) shear layer modes.

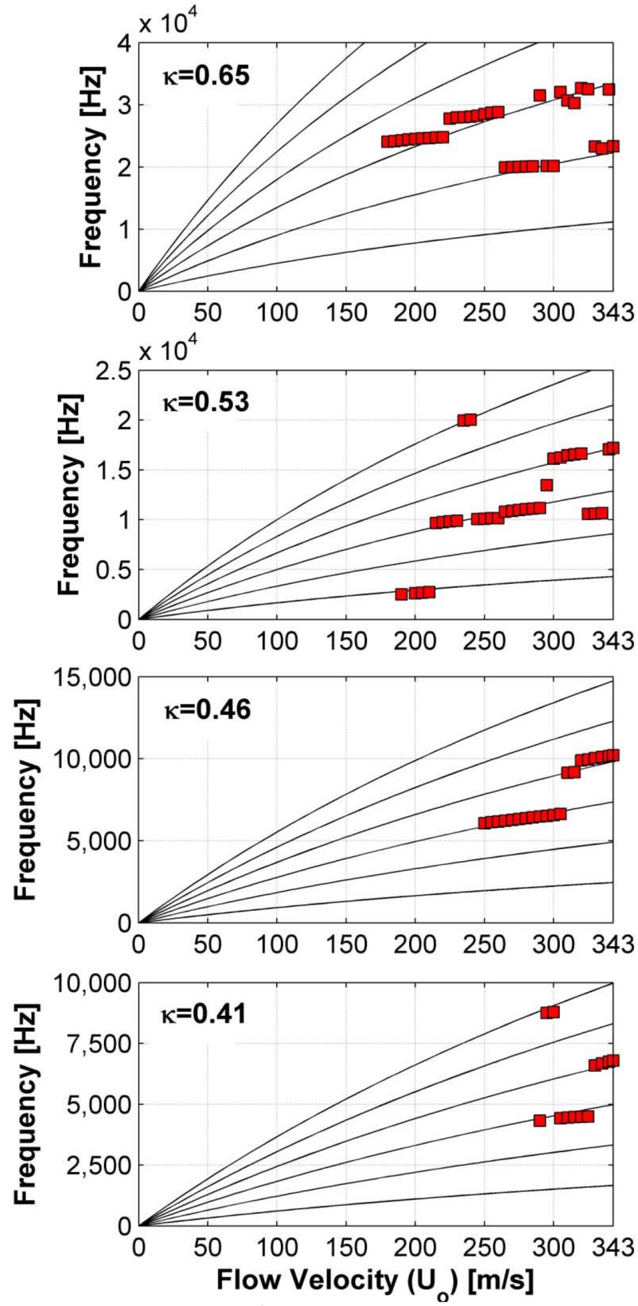

Figure 11: Frequency of the dominant acoustic tones as a function of flow velocity plotted with the prediction of Equation (4) for the n^{th} Rossiter mode for the cases of (*top plot*) z_o/h=6, (*2nd plot*) z_o/h=14, (*3rd plot*) z_o/h=22 & (*bottom plot*) z_o/h=30 for h=2mm.

Extending the Rossiter model to other configurations of the impinging planar jet requires careful consideration of the characteristics of the two different flows. The axisymmetric case has been found to excite tones over a range of impingement ratios from z/D=1.5 to 6, or within the range of the jet's potential core. This means that as the coherent structures are formed and convected between the nozzle and impingement surface, for a significant portion of the impingement distance they are bound by an inner flow stream moving at the speed within the jet's potential core U_o, and the relatively stagnant flow of the entrained flow surrounding the jet. The flow in the potential core of the impinging axisymmetric jet does not experience any significant slowing over the distance from the nozzle to the plate until reaching the impingement zone located very close to the plate, which is not the case for the planar configuration. The planar impinging jet configuration does not begin to generate acoustic tones until it has *exited* the range of the jet's potential core, with tones being generated from z_o/h=6 to z_o/h≈45. This range of impingement ratios, which contains the transitional and self-similar regimes in free planar jet flows, experiences significant bulk slowing of the jet flow, and thus a similar slowing in the speed of the convected structures driving tone generation. For this reason, the velocity scale for the downstream portion of the feedback cycle, given by the term κU_o in Equation (4), needs to be suitably modified to account for this change in structure of the flow between the planar and axisymmetric cases.

Figure 11 shows an extension of the Rossiter model of Equation (4) applied to impingement ratios for the planar case of z_o/h=6 (previously shown), 14, 22 and 30. As the impingement ratio is increased for each successive case shown in the figure, the jet flow experiences a greater bulk slowing effect as it travels from the nozzle to the impingement surface. In order to compensate for this effect, the convection coefficient κ, has been incrementally reduced in each case to obtain the best fit between experimentally measured tone frequencies and the frequencies predicted by the model. Additional impingement ratio cases besides those shown in the figure were also tested, and the complete trend of convection coefficient as a function of the impingement ratio is shown in Figure 12.

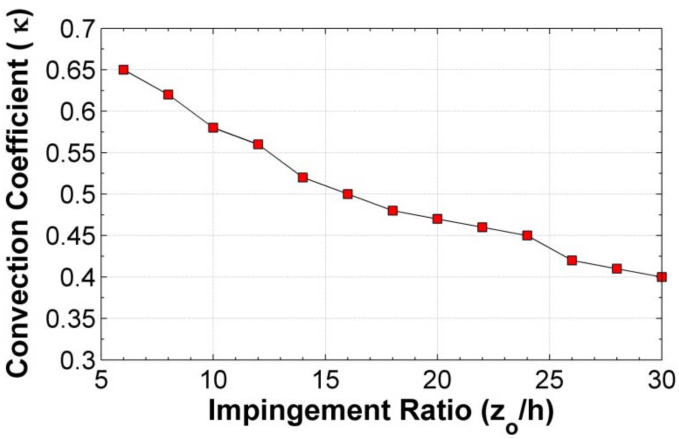

Figure 12: Plot of the convection coefficient (κ) fit to each impingement ratio case tested (*h*=2mm for all cases).

In general it can be seen from Figure 11 that the agreement between the experimentally observed tone frequencies and the prediction of the n^{th} modes of the Rossiter model is quite good. Using the model allows for the identification of the particular shear layer mode which is driving the tone generation for a given configuration. There are several configurations for which there is not a good agreement between the tone frequencies and the model, such as for the impingement ratio case of z_o/h=14 at flow velocities of U_o=295m/s and between U_o=325m/s and 335m/s. Many of these cases appear to correspond to constant frequencies which do not change as the flow velocity increases. These modes are thought to be cases of a jet stage coupling with a resonant acoustic mode of the nozzle plenum, or other geometries in the air supply. A similar coupling was observed by Glesser et al [12] for the jet-edge configuration. Work is currently ongoing to model the plenum and supply using a finite element solver to determine the resonant acoustic modes and assess the source of this discrepancy.

The top plot of Figure 13 shows the frequency of the dominant acoustic tone for four impingement ratio of z_o/h=6, 14, 22 and 30 for a fixed jet slot width of h=2mm. The middle plot non-dimensionalizes the tone frequency of the four cases using the Strouhal number defined by the expression:

$$St_{zo} = \frac{f \cdot z_o}{U_o} \tag{6}$$

where U_o is the flow velocity at the centerline of the jet exiting the nozzle.

It is evident from the figure that the use of this form of the Strouhal number does produce a collapse of the data to some degree, however it is not possible to identify the individual shear layer modes. In addition, there is a clear trend of decreasing Strouhal number with increasing flow velocity. These effects are observed mainly because this form of the Strouhal number uses a single flow velocity corresponding to the exit of the nozzle as the velocity scale, which does not accurately represent the physics of the phenomenon. A more accurate representation of the problem can be obtained by using an effective flow velocity as the velocity scale, which can adequately account for not only the two distinct velocities present for both the upstream and downstream portions of the feedback mechanism, but also for the bulk slowing effect of the planar jet for larger impingement distances. Therefore, the effective flow velocity, U_{eff}, is postulated to have the form given by Equation (7).

$$U_{eff} = \left(U_d + U_u\right)/2 \tag{7}$$

where U_u and U_d are the velocities for the upstream and downstream portions of the feedback mechanism respectively. The upstream velocity U_u, where the acoustic pressure fluctuation travels from the impingement surface to the nozzle exit, is simply the speed of sound, c_a. For the downstream portion of the feedback mechanism, the velocity scale has been selected as the flow velocity at the jet centerline at the midpoint between the nozzle and the impingement surface.

To obtain an estimate of this velocity scale, we have employed the work by Maurel & Solliec [22], who obtained a dimensionless fit for the centerline flow velocity of impinging planar jets for impingement ratios between z_o/h=6 up to 50. The expression given in Equation (8) gives a prediction of the flow velocity along the centerline within the range z/z_o=0.4 up to 0.8.

$$\frac{U_c(z)}{U_o}\sqrt{\frac{z_o}{h}} = -2.9\left(\frac{z}{z_o}\right) + 4.5 \tag{8}$$

Setting the distance downstream to z=0.5z_o and simplifying, the following expression is obtained:

$$U_c\left(z = 0.5 z_o\right) = 3.05 \cdot U_o \sqrt{\frac{h}{z_o}} \tag{9}$$

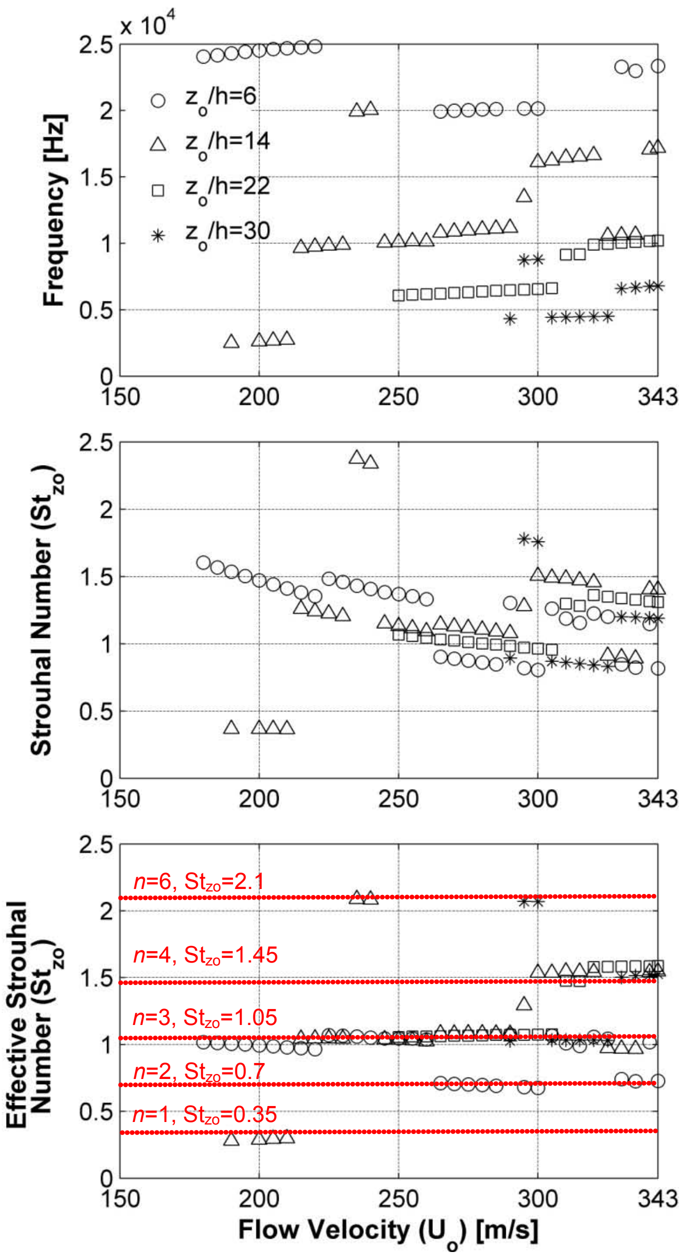

Figure 13: Frequency and Strouhal number (St_{zo}) of the dominant acoustic tone as a function of flow velocity for the cases of z_o/h=6, 14, 22 & 30 for h=2mm.

Using this expression as the downstream velocity U_d, we obtain the following expression for the effective flow velocity, U_{eff}:

$$U_{eff} = \frac{\left(3.05 \cdot U_o \cdot \sqrt{h/z_o}\right) + c_a}{2} \tag{10}$$

The bottom plot of Figure 13 shows the Strouhal number using this effective velocity scale of the dominant acoustic tone as a function of the flow velocity for impingement ratios of z_o/h=6, 14, 22 and 30. It is clear that the Strouhal number utilizing the effective velocity allows for a much more coherent collapse of the data, with the individual shear layer modes being easily identified, which correspond to constant Strouhal numbers as the velocity is varied. The first shear layer mode (n=1) occurs at a Strouhal number of St_{zo}=0.35, with higher shear layer modes occurring at approximately $n \cdot 0.35$ for the 2nd, 3rd, 4th, and 6th shear layer modes respectively.

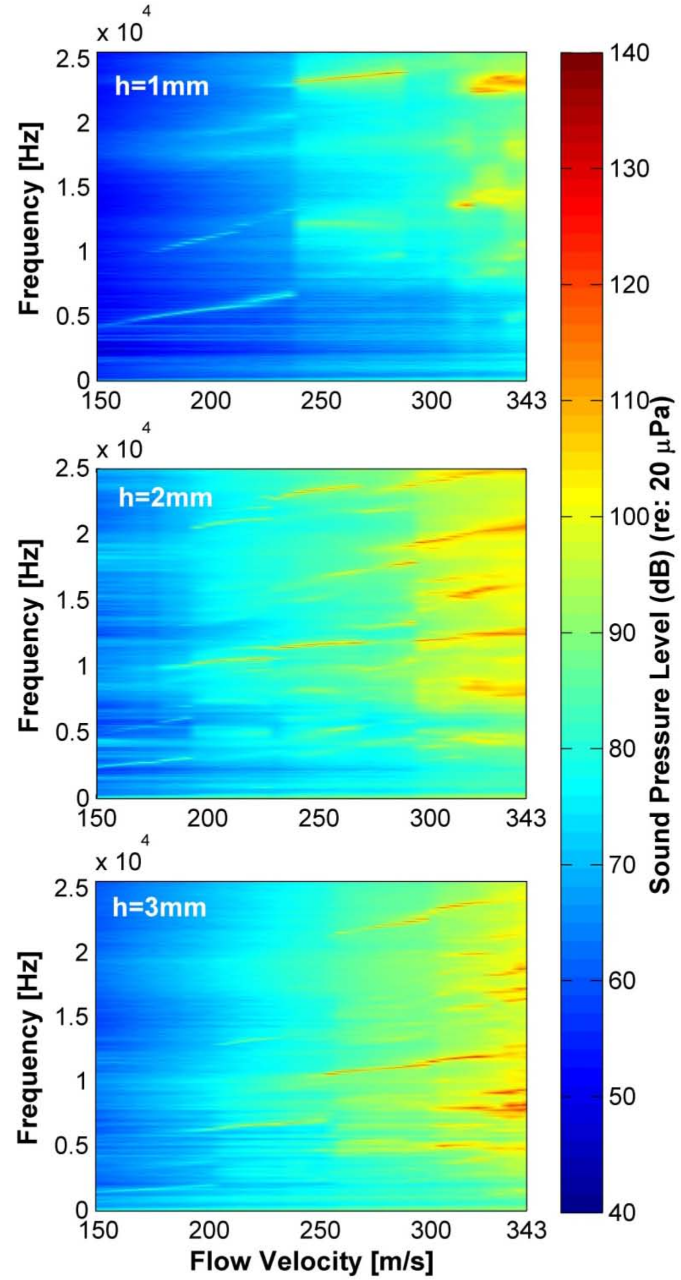

Figure 14: Contour plots showing acoustic spectra as a function of flow velocity for (*top plot*) h=1mm, (*middle plot*) 2mm & (*bottom plot*) 3mm for an impingement ratio of z_o/h=12.

In addition to the cases already presented with a jet slot width of h=2mm, measurements of additional cases with different jet slot widths were also performed. Figure 14 shows a series of contour plots for a fixed impingement ratio of z_o/h=12 and jet slot widths of h=1mm, 2mm and 3mm respectively. The contour plots clearly illustrate that the frequency of the acoustic tones is inversely proportional to the jet slot width, with larger jet slots producing lower frequency tones. In addition, the tones are excited in a similar manner, with the range of impingement ratios for which tones are generated being similar, and in addition, the tones are generated in stages over approximately the same range of flow velocities.

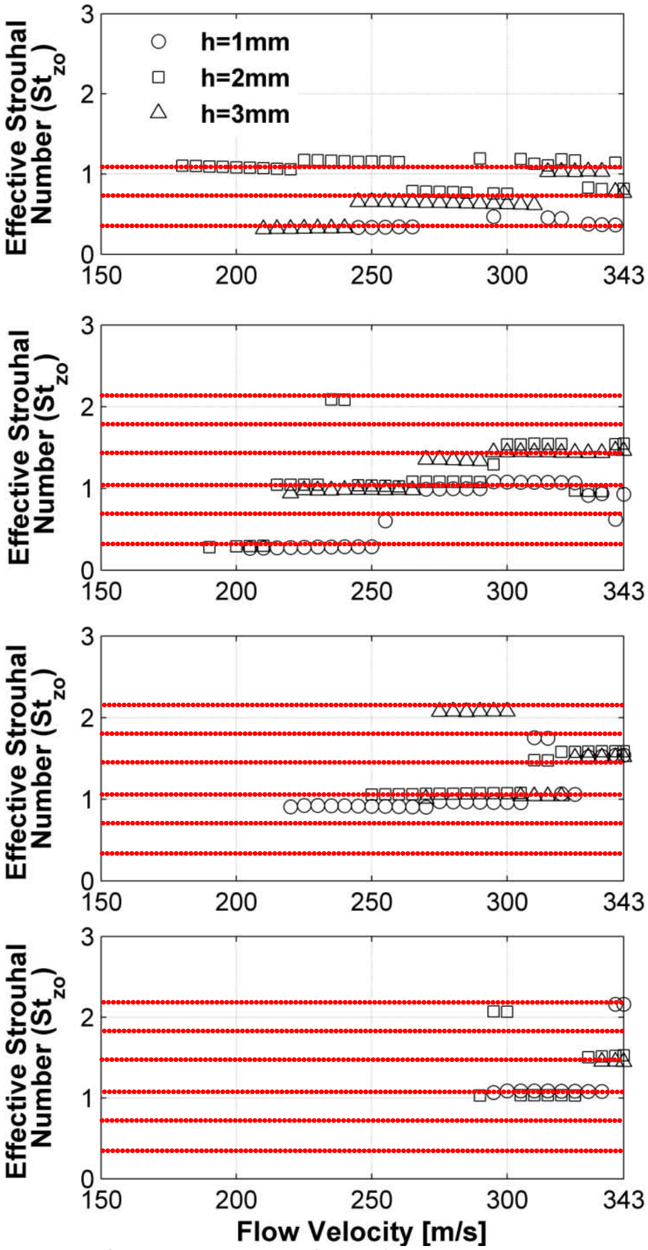

Figure 15: Strouhal number (St_{zo}) of the dominant acoustic tone as a function of flow velocity for h=1mm, 2mm & 3mm, for the cases of (*top plot*) z_o/h=6, (*2nd plot*) z_o/h=14, (*3rd plot*) z_o/h=22 & (*bottom plot*) z_o/h=30.

The contour plots also show that cases with the smallest jet slot width exhibit the lowest levels of broadband noise, and that as the jet slot width is increased, the broadband noise levels rise significantly. This increase in broadband noise levels is thought to be as a result of higher volume flow rates in the nozzle plenum, and decreasing contraction ratio of the nozzle as the jet width is increased, which contributes to increased turbulence intensity of flow impacting the impingement surface. The overall amplitude of the tones themselves also tend to increase as the jet slot width increases, as there is more energy in the flow which can be extracted in the form of acoustic energy.

Figure 15 shows a series of plots showing the Strouhal number using the previously derived effective flow velocity as the velocity scale, and the impingement distance (z_o) as the length scale for three jet slot widths of h=1mm, 2mm and 3mm. The four individual plots show the non-dimensionalized dominant tone frequency for four different impingement ratio cases of z_o/h=6, 14, 22 and 30 respectively. All four plots of the data comparing the three distinct jet slot widths show a good collapse to the n=1 to n=6 shear layer modes, with constant Strouhal numbers as a function of flow velocity.

CONCLUSIONS

The current paper has discussed experimental results of a high speed planar jet impinging on a flat, rigid surface at various flow velocities and distances downstream, and with various jet thicknesses. The geometry has been found to excite intense acoustic tones, excited over various jet stages, for flow velocities of U_o=150m/s, up to choked flow (U_o=343m/s), and for a range of impingement ratios from z_o/h=6 up to as much as z_o/h=45. The tone amplitudes and overall A-weighted sound pressure levels produced by this geometry can be very intense, exceeding 140dB in many cases.

Although the aeroacoustic response of the planar impinging jet system is qualitatively similar to the axisymmetric case, there are a number of distinct differences in the two systems. First, the planar case tends to have a lower critical flow velocity than the axisymmetric case, with tones excited at flow velocities of U_o=150m/s for the planar case, compared to $U_o\approx$205m/s for the axisymmetric configuration. In addition, the range of impingement ratios over which tones are generated is much different for the two cases, with tones being excited within the range of the jet's potential core ($1.5\leq z/D \leq 6.0$), whereas the planar case excites tones only after it has exited this range, with tone excited from z_o/h=6 up to as much as z_o/h=45.

The frequency of these tones was found to be reasonably well predictable using a simple Rossiter model adapted from its application to the axisymmetric jet case, with the modification of adjusting the convection coefficients to account for bulk slowing of the flow for larger impingement ratios. The use of the Rossiter model allows for the identification of the shear layer modes responsible for tone generation. In general it was found that higher shear layer modes were excited for higher flow velocities and larger impingement ratios, which is consistent with both the axisymmetric case, as well as other planar jet cases, such as the jet-edge and jet-slot systems.

Finally, the use of an effective velocity scale, based on both the upstream and downstream portions of the feedback mechanism, results in a more coherent collapse of the data than when using the velocity at the nozzle outlet. It also leads to constant Strouhal numbers of the tones as the flow velocity is increased and thereby easier identification of the various shear layer modes. A good collapse was similarly observed for cases with varying jet slot widths of h=1mm, 2mm and 3mm.

ACKNOWLEDGMENTS

The first author would like to express his appreciation for the generous support of NSERC for funds in support of his Ph.D. program.

REFERENCES

1. O'Donovan, T. S. & Murray, D. B. 2007, "Jet Impingement Heat Transfer – Part I: Mean and Root-Mean-Square Heat Transfer and Velocity Distributions", International Journal of Heat and Mass Transfer, **50,** pp. 3291-3301.

2. O'Donovan, T. S. & Murray, D. B. 2007, "Jet Impingement Heat Transfer – Part II: A Temporal Investigation of Heat Transfer and Local Fluid Velocities", International Journal of Heat and Mass Transfer, **50,** pp. 3302-3314.
3. Ho, C. & Nossier, N. S., 1981, "Dynamics of an Impinging Jet. Part 1. The Feedback Mechanism", Journal of Fluid Mechanics, **105**, pp. 119-142.
4. Nossier, N. S. & Ho, C. 1982, "Dynamics of an Impinging Jet. Part 2, The Noise Generation", Journal of Fluid Mechanics, **116**, pp. 379-391.
5. Tam, C. & Ahuja, K, 1990, "Theoretical Model of Discrete Tone Generation by Impinging Jets", Journal of Fluid Mechanics, **214**, pp. 67-87.
6. Panicker, P. & Raman, R. 2007, "Criteria for the Existence of Helical Instabilities in Subsonic Impinging Jets", Physics of Fluids, **19**, pp. 106103-1.
7. Henderson, B. & Powell, A. 1993, "Experiments Concerning Tones Produced by an Axisymmetric Choked Jet Impinging on Flat Plates", Journal of Sound and Vibration, **168** (2), pp. 307-326.
8. Krothapelli, A., Rajkuperan, E., Alvi, F. & Lourenco, L. 1999, "Flow Field Noise Characteristics of a Supersonic Impinging Jet", Journal of Fluid Mechanics, **392,** pp. 155-181.
9. Henderson, B. 2001, "The Connection Between Sound Production and Jet Structure of the Supersonic Jet", Journal of the Acoustical Society of America, **111** (2), pp. 735-747.
10. Krothapelli, A. 1984, "Discrete Tones Generated by an Impinging Underexpanded Rectangular Jet", AIAA Journal, **23** (12), pp. 1910-1915.
11. Billon, A. Valeau, A. & Sakout, A. 2005, "Two Feedback Paths for a Jet-Slot Oscillator", Journal of Fluids and Structures, **21**, pp. 121-132.
12. Glesser, M. Valeau, A. & Sakout, A. 2008, "Vortex Sound in unconfined flows: Application to the Coupling of a Jet-Slot Oscillator with a resonator", Journal of Sound and Vibration, **314**, pp. 635-649.
13. Rockwell, D. & Naudasher, E. 1979, "Self-Sustained Oscillations of Impinging Free Shear Layers", Annual Review of Fluid Mechanics, **11**, pp. 67–94.
14. Ziada, S. 1995, "Feedback Control of Globally Unstable Flows: Impinging Flows", Journal of Fluids and Structures, **9**, pp. 907-923.
15. Ziada, S. 2001, "Interaction of a Jet-Slot Oscillator with a Deep Cavity Resonator and its Control", Journal of Fluids and Structures, **15**, pp. 831-843.
16. Powell, A. 1961, "On the Edge Tone", Journal of the Acoustical Society of America, **33,** pp. 395-409.
17. Karamcheti, K., Bauer, A.B., Shields, W.L., Stegen, G.R. and Woolley, J.P., 1969, "Some Features of an Edge-Tone Flow Fields", NASA SP-207.
18. Ziada, S. 2002, "Active Stabilization of a Planar Jet Impinging on a Flexible Wedge", Journal of Fluids and Structures **16**, pp. 613-626.
19. Ziada, S. & Rockwell, D. 1982, "Oscillations of an Unstable Mixing Layer Impinging Upon an Edge", Journal of Fluid Mechanics, **124**, pp. 307-334.
20. Hinze, J. O. 1975, Turbulence, 2nd Edition, McGraw Hill Publishing Co.
21. Rossiter, J. E. 1964, "Wind Tunnel Experiments on the Flow Over Rectangular Cavities at Subsonic and Transonic Speeds", Royal Aircraft Establishment, TR No. 64307.
22. Maurel, S. & Solliec, C. 2001, :A turbulent Plane Jet Impinging Near and Far from a Flat Plate", Experiments in Fluids, **31,** pp. 687-696.

